Biosensors and Bioelectronics 32 (2012) 188–194

Contents lists available at SciVerse ScienceDirect

Biosensors and Bioelectronics

journal homepage: www.elsevier.com/locate/bios

# Hydrogen peroxide detection at a horseradish peroxidase biosensor with a Au nanoparticle–dotted titanate nanotube|hydrophobic ionic liquid scaffold

Xiaoqiang Liu [a,**], Heqing Feng [a], Jiamei Zhang [a], Ruoxia Zhao [a], Xiuhua Liu [a], Danny K.Y. Wong [b,*]

[a] Institute of Environmental and Analytical Sciences, College of Chemistry and Chemical Engineering, Henan University, Kaifeng, Henan 475004, PR China
[b] Department of Chemistry and Biomolecular Sciences, Macquarie University, Sydney, NSW 2109, Australia

ARTICLE INFO

*Article history:*
Received 8 September 2011
Received in revised form
29 November 2011
Accepted 1 December 2011
Available online 9 December 2011

*Keywords:*
Gold nanoparticle–dotted $TiO_2$ nanotubes
$TiO_2$–ionic liquid composite materials
Electron transfer of HRP
Detection of $H_2O_2$

ABSTRACT

In this work, a novel sensing scaffold, consisting Au nanoparticle (GNP)–dotted $TiO_2$ nanotubes (TNTs) as the rigid material and the hydrophobic ionic liquid (HIL), 1-decyl-3-methylimidazolium tetrafluoroborate, as the entrapping agent, was applied to facilitate the electron transfer of horseradish peroxidase (HRP) on a glassy carbon electrode. GNPs were immobilised on the TNTs in our work using a one-step reduction of $HAuCl_4{\cdot}3H_2O$ by sodium borohydride in the presence of sodium citrate as a stabilising reagent. The morphology and composition of the as-synthesised composite materials were characterised by transmission electron microscopy, scanning electron microscopy, X-ray diffraction and Fourier-transform infrared spectroscopy. Cyclic voltammetry of HRP at the modified electrode presented a pair of reproducible, quasi-reversible redox peaks with a peak-to-peak separation of 69 mV, indicating electron transfer between HRP and composite electrode. The GNP–TNT|HIL|HRP electrode was then applied to the detection of $H_2O_2$ in a pH 7.0 phosphate buffer using chronoamperometry. The biosensor exhibited a linear response in the 15–750 μM range, and a limit of detection of 2.2 μM. The biosensor also exhibited stability with 90% of the detection signal retained over a two-week duration.



## 1. Introduction

Since the development of the first enzyme-based electrochemical biosensor, much attention has been focused on improvements of their response performances (Hooda et al., 2009; Jamal et al., 2009; Kalimuthu et al., 2010; Miao et al., 2011). However, difficulty of direct electron transfer between the enzyme and the electrode has always been a problem along with the construction of biosensors. This is because the catalytic centre of many enzymes is deeply embedded in an insulating protein shell, resulting in sluggish electron-transfer kinetics (Yin et al., 2009). Moreover, an enzyme generally loses its bioactivity after it is directly adsorbed on an electrode surface (Hong et al., 2006). Therefore, there are continuing demands for development of materials with improved enzyme performance on an electrode surface.

Composite materials have hitherto shown promises in achieving the direct electron transfer of redox enzymes on an electrode (Yu et al., 2011; Zhuo et al., 2011). In assembling such materials, a rigid skeletal component is used to support the entire composite on an electrode surface. Suitable inorganic rigid materials including carbon nanotubes (Arvinte et al., 2010; Bai et al., 2011), ZnO nano materials (Kumar et al., 2009), $TiO_2$ nanoparticles (Cheng et al., 2008; Zhuo et al., 2011) have previously been used to construct electrochemical biosensors. Among them, $TiO_2$ nanoparticles have received increasing attention due to their strong biocompatibility, anti-oxidising properties, chemical inertness, high specific surface area and non-toxicity (Milsom et al., 2007; Shen et al., 2008; Song et al., 2006). In developing $TiO_2$ nanoparticles with improved electrochemical conductivity and an even higher specific surface area, $TiO_2$ nanotubes (TNTs) have been prepared by hydrothermal methods (Kasuga et al., 1998), anodic oxidation (Han et al., 2010) and molecular imprinting methods (Jung et al., 2002). TNTs have been applied to electrochemical and photoelectrochemical developments in recent years (Han et al., 2010; He et al., 2007; Paramasivam et al., 2008). For example, Han et al. constructed a hybrid system consisting of TNTs and poly(amidoamine) dendrimers encapsulated platinum nanoparticles (Pt-DENs) to entrap glucose oxidase (GOx) on a glassy carbon electrode for the electrocatalytic reduction of glucose. An ~11-fold increase in the amperometric responses to glucose was obtained at this biosensor compared with electrodes consisting of GOx in only Pt-DENs. The authors attributed this to the favourable microenvironment of GOx within TNTs, where TNT|Pt-DENs provides a biocompatible environment that retains bioactivity of GOx and facilitates the electron transfer between GOx and electrode.

Another vital component in composite electrode materials is a polymeric entrapping reagent, such as nafion (Liu et al.,

* Corresponding author. Tel.: +61 2 9850 8300; fax: +61 2 9850 8313.
** Corresponding author.
*E-mail address:* Danny.Wong@mq.edu.au (D.K.Y. Wong).

0956-5663/$ – see front matter © 2011 Elsevier B.V. All rights reserved.
doi:10.1016/j.bios.2011.12.002

2011) or chitosan (Khan and Dhayal, 2008), used to immobilise biomolecules, nanoparticles or other materials on an electrode surface. Similar to nafion and chitosan, room temperature ionic liquids are increasingly used as an entrapping reagent in developing different sensors owing to their good biocompatibility, excellent electrical conductivity (1.08–4.38 mS $cm^{-1}$ at 298 K) (Vila et al., 2007; Yu et al., 2009), non-volatility, non-toxicity and a wide electrochemical window (between −1.8 V and 2.4 V at glassy carbon electrodes) (Moganty et al., 2009). For example, Liu et al. developed a GOx biosensor by entrapping GOx and colloidal gold-modified graphite powder in the room temperature ionic liquid, *n*-octyl-pyridinium-hexafluorophosphate. This biosensor showed remarkably strong ability in maintaining the bioactivity and stability of GOx in strongly acidic conditions (pH 2.0) for over an hour. More recently, a screen-printing ink consisting of graphite, cellulose acetate and *n*-octyl-pyridinum-hexafluorophosphate was developed, which was applied to a poly(vinyl chloride) substrate to construct a screen-printed electrode for the detection of dopamine (Ping et al., 2010). The electrode exhibited a linear range between 1.0–2500 μM and a limit of detection of 0.5 μM dopamine. In addition, ionic liquids are also good solvents for nanomaterials by dispersing the nanomaterials without agglomeration. For example, reduction of $PtO_2$ by hydrogen was found to produce isolated platinum nanoparticles without large agglomerates in 1-*n*-butyl-3-methylimidazolium tetrafluoroborate (Scheeren et al., 2008). *In situ* transmission electron microscopic and X-ray diffraction analysis of the samples showed that uniform, 3 nm diameter platinum nanoparticles were produced, with no evidence of bulk metal formation.

In this work, we report the development of a sensing scaffold consisting of Au nanoparticle (GNP)–modified TNTs and the hydrophobic ionic liquid (HIL), 1-decyl-3-methylimidazolium tetrafluoroborate, which was then used to immobilise the enzyme, horseradish peroxidase (HRP), on a glassy carbon electrode to facilitate the electron transfer of HRP. Owing to the similar morphology and structure of TNTs to those of carbon nanotubes used in other composite material-modified electrodes (Gao and Zheng, 2009), TNTs in the GNP–TNT|HIL scaffold act as the rigid skeletal component of a composite material on which the entrapping reagent, HIL, was immobilised. Here, TNTS are decorated with GNPs to improve the electrochemical conductivity of TNTs and hence that of the biosensor. According to Carralero et al. (2006) and Zheng et al. (2011), GNPs would improve the conductivity of TNTs by acting as a conducting tunnel between the heme centres of an enzyme and the electrode surface, which would then aid in enhancing the catalytic effect of HRP on $H_2O_2$ in our work. Moreover, TNTs would not only prevent the aggregation of GNPs, but also offer a biocompatible microenvironment that retains the HRP bioactivity (Han et al., 2010). GNPs were immobilised on the TNTs through a one-step reduction of $HAuCl_4{\cdot}3H_2O$ in a TNT suspension and this was demonstrated to be a simple, low cost and time saving method for the immobilisation procedure. In addition, we have also demonstrated a more efficient treatment for immobilising the composite on an electrode surface. Electrocatalytic response to the reduction of $H_2O_2$ at the GNP–TNT|HIL|HRP-coated electrochemical biosensor was then studied by cyclic voltammetry and amperometry.

## 2. Experimental

### 2.1. Reagents and materials

Hydroquinone (HQ), HRP and $HAuCl_4{\cdot}3H_2O$ were purchased from Sigma–Aldrich, USA. The titanate nanotube material ($Na_2Ti_2O_4(OH)_2$) was prepared using a procedure reported by Yang et al. (2003). In brief, the hydroxyl functionalised titanate nanotube was obtained by reacting polycrystalline $TiO_2$ with concentrated NaOH solution at 110 °C for 20 h. The hydrophobic ionic liquid, 1-decyl-3-methylimidazolium tetrafluoroborate, was obtained from Shanghai Chengjie Chemical Co., Ltd., China. All other reagents were of analytical grade and used without further purification. All solutions were prepared with ultrapure water.

### 2.2. Apparatus

Electrochemical measurements were performed using a CHI630 C electrochemical workstation (Shanghai CH Instruments, China). A conventional three-electrode system consisting of a 3 mm diameter glassy carbon working electrode, a platinum wire counter electrode and a Ag|AgCl (3.0 M KCl) reference electrode was used. All electrodes were purchased from Gaozhiruilian Co. Ltd., Wuhan, China. The working solutions were deoxygenated with nitrogen gas for 15 min before measurements and a nitrogen atmosphere was maintained over the solutions during experiment. The morphological characterisation of Au-TNTs was investigated by field emission transmission electron microscopy (FETEM, Tecnai G2 20, FEI Co. Ltd., USA), X-ray diffraction (XRD, X-PertPro, Netherland) with Cu Kα radiation (λ = 1.5406 nm), and transmission-mode FT-IR (Nicolet 170, USA). The morphological characterisation of the GNP–TNT|HIL and GNP–TNT|HIL|HRP modified electrodes were carried out using scanning electron microscopy (SEM; JSM-7500F, JEOL, Japan).

### 2.3. Preparation of GNP–modified TNTs

We have modified a previously reported (Jana et al., 2001) one-step reduction of $HAuCl_4{\cdot}3H_2O$ precursors to deposit GNPs on the surface of TNTs. In brief, 15.5 mg hydroxyl functionalised TNTs were firstly dispersed in 10 mL ethanol under ultrasonication for 30 min. Next, 20 mL ethanol solution containing 0.63 mM $HAuCl_4{\cdot}3H_2O$ and 1.4 mM sodium citrate was added to the TNTs suspension and stirred sufficiently. Then, 2.4 mL of icy cold, freshly prepared 0.10 M $NaBH_4$ solution (prepared in NaOH solution; pH 12.0) was rapidly added to the above mixture. The mixture was then stirred for an additional 20 h at room temperature. Finally, the mixture was centrifuged, washed with ultrapure water, and dried in a vacuum drying oven at 40 °C.

### 2.4. Preparation of biosensor

GNP–TNT|HIL layer was applied to the glassy carbon electrode by adopting a previously reported procedure (Li et al., 2007; Xiao et al., 2008). Briefly, a glassy carbon electrode was sequentially polished with 0.3 μm and 0.05 μm alumina slurry and sonicated in ultrapure water, ethanol and acetone after each polishing step. An appropriate amount of a ground black paste containing 20 μL HIL and 100 mg GNP–TNTs was applied to only the glassy carbon disc of the electrode. The modified electrode was then immersed in ultrapure water for 10 min and dried in a fume hood. After completely drying, the surface of GNP–TNT|HIL-modified electrode was smoothened with a piece of weighing paper. Next, 10 μL glutaraldehyde was applied to the modified electrode to form a thin dry film, followed by 10 μL HRP and the electrode was dried at 4 °C. This electrode was denoted as a GNP–TNT|HIL|HRP electrode. For comparison, a TNT|HIL|HRP electrode without any GNPs was also fabricated using a similar procedure. The as-prepared electrodes were kept at 4 °C when not in use.

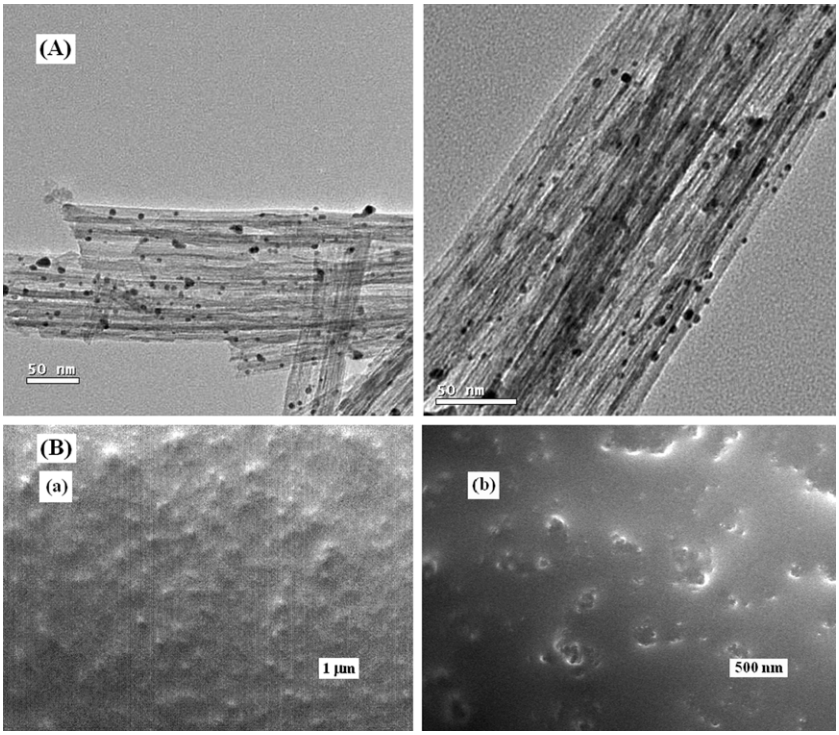


**Fig. 1.** (A) TEM images of GNP–TNT hybrid structures at different orientations. (B) SEM images of the surfaces of the GNP–TNT|HIL (a) and GNP–TNT|HIL|HRP (b) modified electrodes.

## 3. Results and discussion

### 3.1. Spectroscopic characterisation of GNP–TNT|HIL|HRP modified electrodes

Composite materials including carbon nanotubes, ZnO nanomaterials and $TiO_2$ nanoparticles were previously developed for applications such as electrochemical biosensors, modified electrodes and electrochemical immunosensors (Kumar et al., 2009; Yu et al., 2011; Zhuo et al., 2011). In exploiting the advantages of TNTs stated in Introduction, we have applied in this work TNTs as the rigid material and HIL as the entrapping reagent in developing a novel composite material for immobilisation of enzyme on a biosensor surface. As demonstrated later, such a biosensor facilitates the electron transfer of HRP and achieves improved analytical performance for the determination of $H_2O_2$. We have initially characterised GNP–modified TNTs using TEM, XRD, and FT-IR. In Fig. 1(A), the TEM images of the as-prepared GNP–TNTs illustrate that the TNTs fabricated in our work have nearly uniform diameters of approximately 100 nm and lengths over 300 nm. On the other hand, well-dispersed, spherical gold particles with diameters of 5–7 nm anchored on the external walls of TNTs are clearly visible in all these images, which demonstrated the feasibility of the immobilisation method of GNPs on TNTs. The average particle size is approximately 5.3 nm and this estimation is consistent with those obtained from XRD data presented below.

Next, SEM was conducted to characterise the GNP–TNT|HIL and GNP–TNT|HIL|HRP electrodes. The SEM image (a) in Fig. 1(B) shows a relatively even and smooth GNP–TNT|HIL layer on the electrode. However, both TNTs and GNPs are indiscernible on this sensing layer due to a blanketing effect and dispersing ability of the viscous HIL. After immobilising HRP on the GNP–TNT|HIL electrode, the corresponding SEM image (b) reveals some bright island-like aggregates regularly distributed on the composite sensing layer. These island-like aggregates are most likely attributable to the three-dimensional structure of enzyme molecules. Previous work (Yu and Ju, 2002; Zhang et al., 2009; Zhou and Zhi, 2006) reported that such morphology of enzyme-modified electrodes aided in increasing the catalytic effect of enzyme on the substrate, which would be beneficial to the analytical performance of the enzyme biosensors.

XRD was also used to study the bulk structure of GNP–decorated TNTs discussed above and the results are shown in Fig. 2(a). As previously reported (Han et al., 2010), the strong diffraction peaks at $2\theta$ angles of 25.0°, 37.4° and 48.5° may be assigned to the spacing of (1 0 1), (0 0 4) and (2 0 0) of the anatase (tetragonal) phase of the TNTs. Similar to those previously reported (Paramasivam et al., 2008; Song et al., 2010), major diffraction peaks of GNPs are also clearly observed at 37.8°, 45.0°, 65.0° and 78.0°, which can be assigned to (1 1 0), (2 0 0), (2 2 0), (3 1 1) reflection of Au, respectively. Based on these XRD results, the average Au particle size ($d$) can be estimated using the Scherrer equation (Park et al., 2002; Yang et al., 2005),

$$d = \frac{0.9 \times \lambda_{K\alpha}}{B_{(2\theta)}\cos\theta_{max}}$$

where $\lambda_{K\alpha}$ is the wavelength of X-rays used (0.154056 nm), $B_{(2\theta)}$ is the width of the peak at the half height (with the peak height evaluated from the baseline), and $\theta_{max}$ is the Bragg angle at the peak. In this manner, $d$ was estimated to be 5.4 nm, which is in good agreement with the average particle size (5.3 nm) estimated from TEM image above.

FT-IR spectra of TNTs and GNP–TNTs are displayed as trace (i) and (ii), respectively, in Fig. 2(b). In trace (i), the band observed at 3390 $cm^{-1}$ is assigned to the stretching of a hydroxyl group chemisorbed on a surface defect site. The band at 1623 $cm^{-1}$, pertaining to H–O–H bending for molecular water, was also observed. This is a clear indication that molecular water adsorption occurred on the surface of TNTs and hydroxyl groups were produced by water dissociation in heating the physisorbed layer as outlined in Section 2.1 (Linsebigler et al., 1995). The absorption band at 1380 $cm^{-1}$ represents the symmetric bending of $CH_3$ groups. The band at 500 $cm^{-1}$

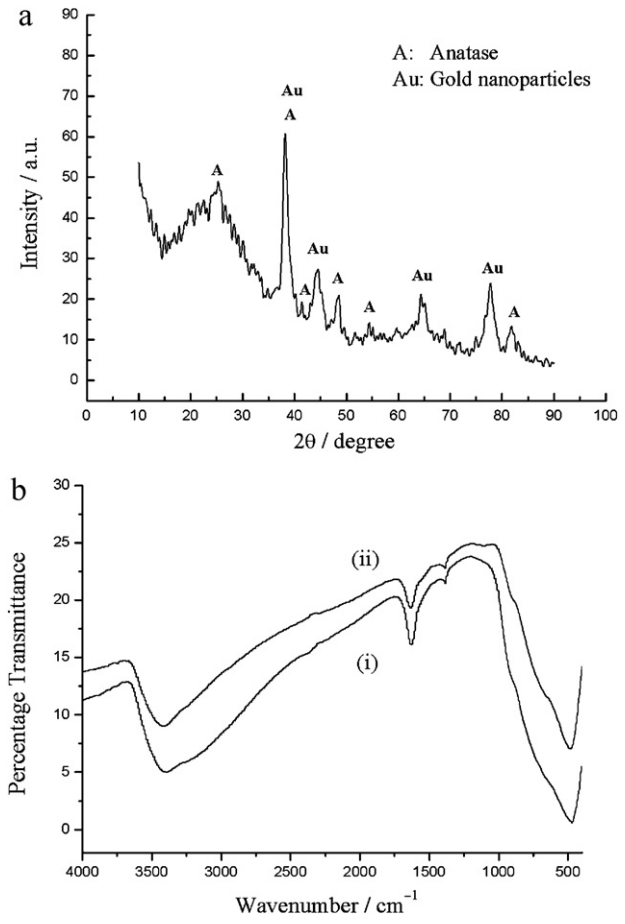


**Fig. 2.** (a) XRD pattern of the GNP–TNTs; (b) FT-IR spectra of TNTs and the GNP–TNT composite.

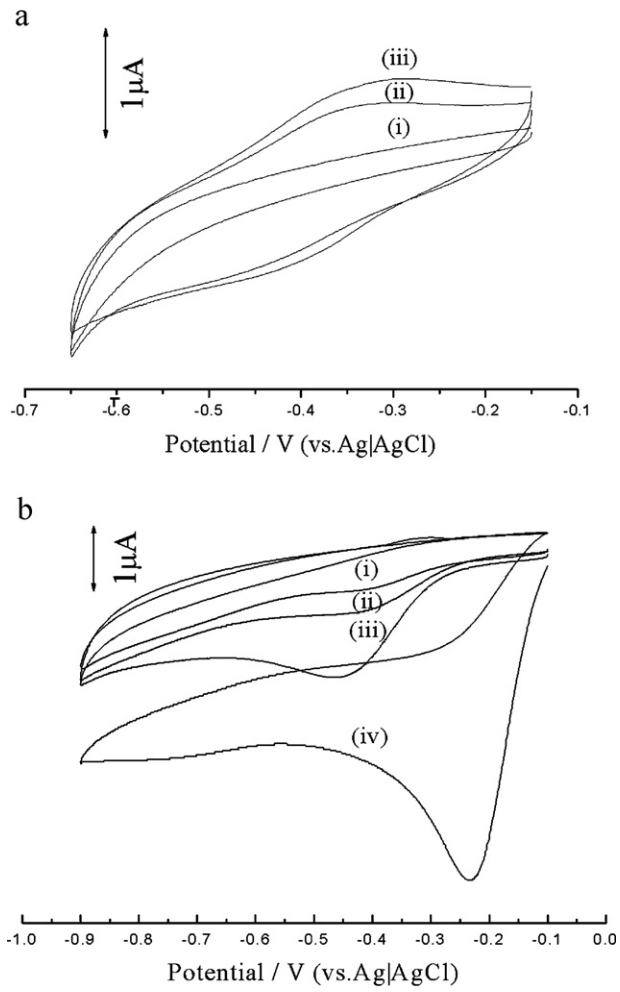


**Fig. 3.** (a) Cyclic voltammograms of (i) GNP–TNT|HIL electrode; (ii) TNT|HIL|HRP electrode; (iii) GNP–TNT|HIL|HRP electrode in 0.05 mol $L^{-1}$ PBS (pH 7.0) at 50 mV $s^{-1}$; (b) cyclic voltammograms of the GNP–TNT|HIL|HRP biosensor in 0.05 mol $L^{-1}$ PBS (pH 7.0) containing (i) 0.1 mmol $L^{-1}$, (ii) 0.3 mmol $L^{-1}$, (iii) 3.0 mmol $L^{-1}$ and (iv) 3.0 mmol $L^{-1}$ $H_2O_2$ and 0.5 mmol $L^{-1}$ HQ at 50 mV $s^{-1}$.

is associated with the Ti–O–Ti stretching mode of $TiO_2$ (Lu and Yang, 2009). The FT-IR spectrum of GNP|TNTs shown in trace (ii) is similar to that of pure TNTs in trace (i), except that that the OH stretching band of GNP|TNTs in trace (ii) has increased by 30 $cm^{-1}$ compared with that in trace (i). This shift is most likely caused by the strong interaction between GNPs and the OH groups of TNTs (Xu et al., 2005).

The TEM, XRD and FT-IR results above provided evidence for the successful immobilisation of GNPs on the TNT surface. Notably, the results shown in Figs. 1(A) and 2 were obtained after the GNP–immobilised TNTs were subjected to washing, purification and drying, indicating the high stability of the composite even after all the treatments. In immobilisation methods reported so far (Kiss et al., 2011; Mendez-Cruz et al., 2011), GNP–modified TNTs must first be obtained by deposition–precipitation with urea, followed by several additional steps including heating to 80 °C for 16 h, stirring in 50 mL of distilled water at 50 °C, centrifuging at 50 °C, and drying under vacuum at 80 °C for 2 h and storing away from light in a desiccator under vacuum. Moreover, these treatment steps must be repeated four times before the GNP–modified TNTs were ready for use. In contrast, preparation of GNP–modified TNTs was achieved in a relatively simple and mild condition in this work. Our results thus demonstrated the one-step reduction method as an effective, simple, low cost and time saving immobilisation strategy.

### 3.2. Electrochemistry of HRP at GNP–TNT|HIL modified electrode

Fig. 3(a) shows the cyclic voltammograms obtained at different modified electrodes: (i) the GNP–TNT|HIL electrode; (ii) the TNT|HIL|HRP electrode; (iii) the GNP–TNT|HIL|HRP electrode in 0.05 mol $L^{-1}$ phosphate-buffered saline (PBS) at pH 7.0 at a scan rate of 50 mV $s^{-1}$. There are no observable redox peaks in the cyclic voltammogram obtained at the GNP–TNT|HIL electrode (trace (i)), indicating neither GNP–TNTs nor HIL was electrochemically active between −0.15 V and −0.65 V. This composite scaffold was therefore not expected to interfere with subsequent electrochemical detection. On the other hand, a pair of redox peaks at approximately −0.35 V and −0.43 V was observed in the cyclic voltammogram obtained at the TNT|HIL|HRP-modified electrode (trace (ii)). Similar cyclic voltammetric peaks were previously observed when cyclic voltammetry of HRP was conducted at gold nano-seed–dotted $TiO_2$ nanoparticles modified glassy carbon electrode (Wang et al., 2010; Yin et al., 2009) and the peaks were attributed to the Fe(III)/Fe(II) redox couple of the heme protein of HRP. Based on the average of these two peaks, the formal potential was determined to be −0.39 V. In our work, the application of a TNT-HIL composite enhanced the biocompatibility and provided a favourable microenvironment for HRP, which aided in retaining the bioactivity of HRP and facilitating the direct electron transfer between HRP and electrode. Furthermore, the HIL increased (by approximately 200% compared with modified electrodes without HIL) the electrical conductivity of the modified electrode, which is also beneficial to the direct electrochemistry of HRP. We speculate that the amphiphlic

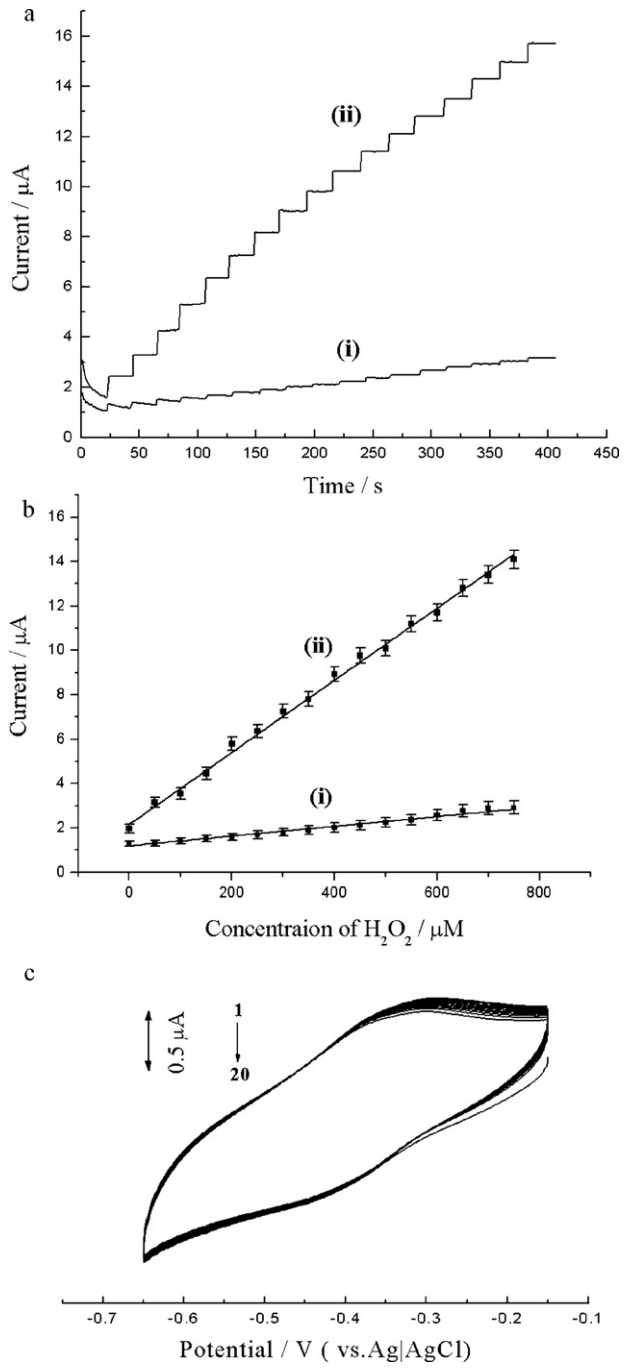


**Fig. 4.** (a) Typical amperometric response of the GNP–TNT|HIL|HRP biosensor in (i) the absence and (ii) presence of 0.1 mmol $L^{-1}$ HQ with additions $H_2O_2$ in 0.05 mol $L^{-1}$ PBS (pH 7.0) at the operating potential of −0.4 V; (b) corresponding calibration plots for the GNP–TNT|HIL|HRP biosensor (same experimental conditions as Fig. 4(a)); (c) twenty times repetitive cyclic voltametric scans of the GNP–TNT|HIL|HRP biosensor in 0.05 mol $L^{-}$ PBS (pH 7.0) at a scan rate of 50 mV $s^{-1}$.

character of HIL would have also improved the functionality of HRP in the system, because there was no diminished catalytic activity or denature of HRP observed even in the hydrophobic environment of HIL used in our work (Yan et al., 2007; Zhou et al., 2008).

Next, cyclic voltammetry was carried out at a GNP–TNT|HIL|HRP-modified electrode and the result is shown in trace (iii). An approximately 22% larger redox peak current was obtained compared with that on a TNT|HIL|HRP-modified electrode. In addition, the peak separation between anodic and cathodic peak decreased by 10 mV compared to that displayed in the cyclic voltammogram obtained at the TNT|HIL|HRP-modified electrode. Clearly, the synergistic effects of the GNP, HIL and TNT composite have yielded improved voltammetric response of HRP at the GNP–TNT|HIL film over that of TNT|HIL by enhancing the biocompatibility of the composite and the electrical conductivity of the modified electrodes.

The effect of potential scanning rate on the response of GNP–TNT|HIL|HRP electrodes was also investigated. Our results (data not included) showed that the redox peak currents increased linearly with scan rate from 50 to 500 mV $s^{-1}$. The peak-to-peak separation also increased with the increase of the scan rates. These results support a quasi-reversible redox reaction with a surface-controlled process.

### 3.3. Electrochemical response of the GNP–TNT|HIL|HRP biosensor to $H_2O_2$

The catalytic reduction of 0.1, 0.3 and 3.0 mmol $L^{-1}$ $H_2O_2$ at a GNP–TNT|HIL|HRP-modified electrode was initially studied and the results are shown in trace (i), (ii) and (iii), respectively, in Fig. 3(b). As expected, the reduction peak current at approximately −0.41 V in these traces increased at the GNP–TNT|HIL|HRP electrode with increasing $H_2O_2$concentration, accompanied by a decrease of the oxidation peak current at approximately −0.32 V. This result can be explained by the catalytic mechanism of the immobilised HRP for $H_2O_2$ reduction, which is represented by the following scheme proposed by Yi et al. (2000):

$$\mathrm{HRP(Fe^{3+})} + \mathrm{H_2O_2} \rightarrow \mathrm{Compound\ I\ (Fe^{4+}{=}O)} + \mathrm{H_2O} \quad (1)$$

$$\mathrm{Compound\ I\ (Fe^{4+}{=}O)} + \mathrm{e^-} + \mathrm{H^+} \rightarrow \mathrm{Compound\ II} \quad (2)$$

$$\mathrm{Compound\ II} + \mathrm{e^-} + \mathrm{H^+} \rightarrow \mathrm{HRP(Fe^{3+})} + \mathrm{H_2O} \quad (3)$$

where "$Fe^{4+}$=O" denotes oxyferrite. In this scheme, HRP is oxidised by $H_2O_2$ to form an intermediate (Compound I), which consists of oxyferrylheme and a porphyrincation radical. The porphyrin radical of Compound I accepts one electron from the electrode and is reduced to a second intermediate (Compound II), which is subsequently reduced back to the native HRP by accepting another electron from the electrode. Notably, in the absence of $H_2O_2$, the redox reaction of heme in HRP is that between HRP($Fe^{3+}$) and HRP($Fe^{2+}$):

$$\mathrm{HRP(Fe^{3+})} + \mathrm{e} \rightleftharpoons \mathrm{HRP(Fe^{2+})}$$

In the presence of $H_2O_2$, HRP($Fe^{3+}$) reacts to form Compound I and Compound II. Therefore, the electrochemical reduction of both Compound I and Compound II would produce a larger current than the reduction of HRP($Fe^{3+}$) alone. However, as there is no direct involvement of HRP($Fe^{2+}$) in reactions (1)–(3) above, a diminishing oxidation current of HRP($Fe^{2+}$) was observed.

To further improve the analytical performance of the proposed $H_2O_2$ biosensor, HQ was added as an electron mediator. Trace (iv) in Fig. 3(b) depicts the cyclic voltammogram of a GNP–TNT|HIL|HRP-modified electrode in a pH 7.0 PBS (0.05 mol $L^{-1}$) containing 0.5 mmol $L^{-1}$ HQ and 3.0 mmol $L^{-1}$ $H_2O_2$. The catalytic peak current for $H_2O_2$ reduction was found to be over 160% higher than that in the absence of HQ (trace (iii) in Fig. 3(b)), indicating improved sensitivity of the proposed biosensor in the presence of HQ. The sensitivity enhancement by HQ can be explained by the following reaction mechanism (Chen et al., 2006):

$$\mathrm{HRP(Fe^{3+})} + \mathrm{HQ(red)} \rightarrow \mathrm{HRP(Fe^{2+})} + \mathrm{HQ(ox)} \quad (4)$$

$$\mathrm{HRP(Fe^{2+})} + \mathrm{H_2O_2} \rightarrow \mathrm{HRP(Fe^{3+})} + \mathrm{H_2O} \quad (5)$$

$$\mathrm{HQ(ox)} + \mathrm{e^-} \rightarrow \mathrm{HQ(red)} \quad (6)$$

**Table 1**
Analytical performance of different $H_2O_2$ biosensors.

| HRP biosensors | Dynamic range ($\mu$mol L$^{-1}$) | Limit of detection ($\mu$mol L$^{-1}$) | Response time (s) | References |
|---|---|---|---|---|
| GNP–TNT\|HIL\|HRP biosensor | 15–750 | 2.2 | 3 | This work |
| Nafion\|HRP–gold nanoseeds–$TiO_2$\|glassy carbon electrode | 41–630 | 5.9 | 3 | Wang et al. (2010) |
| Haemoglobin\|carboxymethyl cellulose–$TiO_2$–NTs\|glassy carbon electrode | 4–64 | 4.6 | 10 | Zheng et al. (2008) |
| HRP\|Au\|$TiO_2$\|Ti | 5–400 | 2.0 | 5 | Kafi et al. (2008) |
| HRP–$TiO_2$\|pyrolytic graphite electrode | 7.5–123 | 2.5 | Not reported | Zhang et al. (2004) |

Firstly, HRP($Fe^{3+}$) is reduced by HQ(red) to produce HRP($Fe^{2+}$). Then, as shown in reaction (5), HRP($Fe^{3+}$) is regenerated with the help of $H_2O_2$. Finally, HQ(ox) is electrochemically reduced on the electrode surface to produce an electrochemical signal. Therefore, the presence of mediator HQ has further enhanced the reduction current of HRP($Fe^{3+}$).

The amperometric response of GNP–TNT|HIL|HRP-modified electrodes at an applied potential of −0.4 V with successive additions of $H_2O_2$ to PBS (pH 7.0) is shown in Fig. 4. For comparison, Fig. 4(a) presents the typical amperometric response of the GNP–TNT|HIL|HRP biosensor in the absence of HQ (i) and in the presence of 1.0 mmol L$^{-1}$ HQ (ii). The corresponding calibration plots for the two amperometric systems are shown in Fig. 4(b). In the presence of HQ, the calibration plot between 15 and 750 $\mu$mol L$^{-1}$ $H_2O_2$ can be represented by the linear relationship (with a statistical significant correlation coefficient of 0.994 at the 95% confidence level):

$$\text{peak current}\,(\mu\text{A}) = (16.1 \pm 0.26) \times 10^{-3}(\mu\text{A}\,\mu\text{M}^{-1})[H_2O_2] + 2.26 \pm 0.14$$

where the errors denote 95% confidence intervals. Similarly, the corresponding calibration plot (with a correlation coefficient of 0.996) obtained in the absence of HQ is represented by

$$\text{peak current}\,(\mu\text{A}) = (2.35 \pm 0.062) \times 10^{-3}(\mu\text{A}\,\mu\text{M}^{-1})[H_2O_2] + 1.15 \pm 0.09$$

Clearly, the presence of HQ significantly increases the amperometric response of the GNP–TNT|HIL|HRP biosensor (the slopes of plots (i) and (ii) are $2.35 \times 10^{-3}$ and $16.1 \times 10^{-3}$ $\mu$A $\mu$M$^{-1}$, respectively). As shown in (ii) of Fig. 4(a), over 95% of the steady-state current at the GNP–TNT|HIL|HRP biosensor was achieved within 3 s in the presence of HQ. Based on a signal-to-noise ratio of 3, the limit of detection was estimated to be 2.2 $\mu$mol L$^{-1}$. The GNP–TNT|HIL|HRP biosensor developed in this study shows superiority over other $H_2O_2$ biosensors (Yu and Ju, 2002; Wang et al., 2010; Zhang et al., 2004; Zheng et al., 2008) in terms of dynamic range, limit of detection and response time, as tabulated in Table 1.

### 3.4. Stability and precision of the biosensor

In constructing most ionic liquid-modified electrodes, the ionic liquid was initially mixed with carbon nanotubes by sonication. The dispersion was then applied to an electrode, before the electrode was air-dried (Pauliukaite et al., 2011; Zhu et al., 2011). Such a preparation method requires a substantial drying time and also often results in loss of modified materials during the subsequent tests. In contrast, the procedure in our work involves applying a fixed amount of HIL–GNPs–TNTs on a glassy carbon electrode and then immersing the modified electrode in ultrapure water for 10 min before being dried. This immersion treatment was demonstrated to be a rapid, effective step for immobilising GNPs–TNTs on the electrode surface. The stability of the GNP–TNT|HIL|HRP biosensor was next investigated. As shown in Fig. 4(c), no significant change (<5%) in the cyclic voltammetric responses was observed even after repeating 20 continuous scans between −0.15 V and −0.65 V at 50 mV s$^{-1}$. In studying the long-term stability of this biosensor, GNP–TNT|HIL|HRP modified electrodes were stored in small vials and kept at 4 °C when not in use. In this way, the electrodes still yielded 90% of the initial current response after two weeks, compared to a corresponding 65% without adopting our immersion treatment. The reason for the better stability can be attributed to the fast and more complete gelation of the GNP–TNT|HIL composite on the electrode after a 10 min immersion in ultrapure water. We are unclear of the mechanism for the above result, but some specific interaction between water molecules and HIL might be responsible for the fast and complete gelation of HIL. Of course, subsequent evaporation of water during drying in fume hood would have also accelerated the formation of the HIL composite. In terms of repeatability, a relative standard deviation of 3.7% was estimated after 10 successive measurements at a $H_2O_2$ concentration of 0.1 mmol L$^{-1}$. Precision was also studied based on results obtained at six HRP biosensors (fabricated in a single batch) in 0.1 mmol L$^{-1}$ $H_2O_2$. A relative standard deviation of 4.6% was obtained, indicating a high degree of fabrication reproducibility of the biosensor.

### 3.5. Interference study and real-life sample analysis

The selectivity of the biosensor was investigated by detecting $H_2O_2$ (0.1 mmol L$^{-1}$) in the presence of several possible coexisting interferences such as uric acid, ascorbic acid, dopamine, cysteine and glucose at a concentration level of 0.2 mmol L$^{-1}$. As shown in Table 2a, the amperometric response change was found to be less than 10%, after spiking 0.2 mM interferences motioned above, respectively, into 0.1 mM $H_2O_2$ in 0.05 mol L$^{-1}$ PBS (pH 7.0). This result demonstrated high selectivity and anti-interference ability at the biosensor consisting of a GNP–TNT|HIL|HRP scaffold. Next, the analytical performance of the GNP–TNT|HIL|HRP biosensor was evaluated by quantitatively determining $H_2O_2$ in some local disinfectant samples. These disinfectant samples were diluted 100 times before detection and the analytical results are displayed in Table 2b. The recoveries for spiked real-life samples at three different levels

**Table 2a**
Effects of possible interferents on the biosensor response.

| Interferents | % Response | Relative standard deviation ($n$ = 4) |
|---|---|---|
| Uric acid | 93.6 | 1.61% |
| Ascorbic acid | 95.3 | 1.95% |
| Dopamine | 107.4 | 1.84% |
| Cysteine | 96.5 | 1.69% |
| Glucose | 101 | 1.88% |

**Table 2b**
Detection of $H_2O_2$ in disinfectant samples.

| Sample | Added (mM) | Found (mM) | Recovery | Relative standard deviation |
|---|---|---|---|---|
| 1 | 0.100 | 0.106 | 106% | 2.1% |
| 2 | 0.150 | 0.143 | 95.3% | 2.9% |
| 3 | 0.200 | 0.204 | 102% | 3.7% |

are all found to lie in the range of 95.3–106%, demonstrating the feasibility of the biosensor for the detection of $H_2O_2$ in real-life samples.

## 4. Conclusions

In the present work, we have developed a composite film consisting of GNP–modified TNTs and the hydrophobic ionic liquid, 1-decyl-3-methylimidazolium tetrafluoroborate, which facilitates the electrochemistry of HRP at a glassy carbon electrode. The GNP–TNTs exhibit a large surface area and good biocompatibility, providing microenvironment with improved conductivity for the redox activity of HRP. In summary, the biosensor based on the GNP–TNT|HIL|HRP biocomposite film shows such characteristics as ease of fabrication, low cost, fast response, high sensitivity and good stability. The GNP–TNT|HIL|HRP biosensor exhibits a dynamic range between 15 μM and 750 μM, with a 2.2 μM limit of detection and a 3 s response time for the detection of $H_2O_2$.

## Acknowledgements

This work was supported by the International Science and Technology Cooperation Program of Henan Science and Technology Department (084300510023) and the Key Technology Research and Development Program of Henan Science and Technology Department (092102310282).

## References

Arvinte, A., Westermann, A.C., Sesay, A.M., Virtanen, V., 2010. Sens. Actuators B 150, 756–763.
Bai, Y.-C., Zhang, W.-D., Chen, C.-H., Zhang, J.-Q., 2011. J. Alloys Compd. 509, 1029–1034.
Carralero, V., Mena, M.L., Gonzalez-Cortes, A., Yanez-Sedeno, P., Pingarron, J.M., 2006. Biosens. Bioelectron. 22, 730–736.
Chen, S., Yuan, R., Chai, Y., Xu, L., Wang, N., Li, X., Zhang, L., 2006. Electroanalysis 18, 471–477.
Cheng, J., Di, J., Hong, J., Yao, K., Sun, Y., Zhuang, J., Xu, Q., Zheng, H., Bi, S., 2008. Talanta 76, 1065–1069.
Gao, R., Zheng, J., 2009. Electrochem. Commun. 11, 608–611.
Han, X., Zhu, Y., Yang, X., Li, C., 2010. J. Alloys Compd. 500, 247–251.
He, B.-L., Dong, B., Li, H.-L., 2007. Electrochem. Commun. 9, 425–430.
Hong, J., Ghourchian, H., Moosavi-Movahedi, A.A., 2006. Electrochem. Commun. 8, 1572–1576.
Hooda, V., Gahlaut, A., Kumar, H., Pundir, C.S., 2009. Sens. Actuators B 136, 235–241.
Jamal, M., Worsfold, O., McCormac, T., Dempsey, E., 2009. Biosens. Bioelectron. 24, 2926–2930.
Jana, N.R., Gearheart, L., Murphy, C.J., 2001. Langmuir 17, 6782–6786.
Jung, J.H., Kobayashi, H., van Bommel, K.J.C., Shinkai, S., Shimizu, T., 2002. Chem. Mater. 14, 1445–1447.
Kafi, A.K.M., Wu, G., Chen, A., 2008. Biosens. Bioelectron. 24, 566–571.
Kalimuthu, P., Tkac, J., Kappler, U., Davis, J.J., Bernhardt, P.V., 2010. Anal. Chem. 82, 7374–7379.
Kasuga, T., Hiramatsu, M., Hoson, A., Sekino, T., Niihara, K., 1998. Langmuir 14, 3160–3163.
Khan, R., Dhayal, M., 2008. Electrochem. Commun. 10, 263–267.
Kiss, J., Ovari, L., Oszko, A., Potari, G., Toth, M., Baan, K., Erdohelyi, A., 2011. Catal. Today, doi:10.1016/j.cattod.2011.06.002(in press, Corrected Proof).
Kumar, A.S., Cheng, H.-W., Chen, S.-M., 2009. React. Funct. Polym. 69, 364–370.
Li, J., Zhao, F., Zeng, B., 2007. Microchim. Acta 157, 27–33.
Linsebigler, A.L., Lu, G., Yates, J.T., 1995. Chem. Rev. 95, 735–758.
Liu, X., Feng, H., Liu, X., Wong, D.K.Y., 2011. Anal. Chim. Acta 689, 212–218.
Lu, M.-D., Yang, S.-M., 2009. J. Colloid Interface Sci. 333, 128–134.
Mendez-Cruz, M., Ramirez-Solis, J., Zanella, R., 2011. Catal. Today 166, 172–179.
Miao, P., Ning, L., Li, X., Shu, Y., Li, G., 2011. Biosens. Bioelectron. 27, 178–182.
Milsom, E.V., Novak, J., Oyama, M., Marken, F., 2007. Electrochem. Commun. 9, 436–442.
Moganty, S.S., Baltus, R.E., Roy, D., 2009. Chem. Phys. Lett. 483, 90–94.
Paramasivam, I., Macak, J.M., Schmuki, P., 2008. Electrochem. Commun. 10, 71–75.
Park, K.-W., Choi, J.-H., Kwon, B.-K., Lee, S.-A., Sung, Y.-E., Ha, H.-Y., Hong, S.-A., Kim, H., Wieckowski, A., 2002. J. Phys. Chem. B 106, 1869–1877.
Pauliukaite, R., Doherty, A.P., Murnaghan, K.D., Brett, C.M.A., 2011. J. Electroanal. Chem. 656, 96–101.
Ping, J., Wu, J., Ying, Y., 2010. Electrochem. Commun. 12, 1738–1741.
Scheeren, C.W., Domingos, J.B., Machado, G., Dupont, J., 2008. J. Phys. Chem. C 112, 16463–16469.
Shen, Q., You, S.-K., Park, S.-G., Jiang, H., Guo, D., Chen, B., Wang, X., 2008. Electroanalysis 20, 2526–2530.
Song, M., Pan, C., Li, J., Wang, X., Gu, Z., 2006. Electroanalysis 18, 1995–2000.
Vila, J., Varela, L.M., Cabeza, O., 2007. Electrochim. Acta 52, 7413–7417.
Wang, Y., Ma, X., Wen, Y., Xing, Y., Zhang, Z., Yang, H., 2010. Biosens. Bioelectron. 25, 2442–2446.
Xiao, F., Zhao, F., Li, J., Liu, L., Zeng, B., 2008. Electrochim. Acta 53, 7781–7788.
Xu, J.-Z., Zhao, W.-B., Zhu, J.-J., Li, G.-X., Chen, H.-Y., 2005. J. Colloid Interface Sci. 290, 450–454.
Yan, R., Zhao, F., Li, J., Xiao, F., Fan, S., Zeng, B., 2007. Electrochim. Acta 52, 7425–7431.
Yang, H., Coutanceau, C., Leger, J.-M., Alonso-Vante, N., ClaudeLamy, 2005. J. Electroanal. Chem. 576, 305–313.
Yang, J., Jin, Z., Wang, X., Li, W., Zhang, J., Zhang, S., Guo, X., Zhang, Z., 2003. Dalton Trans. 20, 3898–3901.
Yi, X., Ju, H.-X., Chen, H.-Y., 2000. Anal. Biochem. 278, 22–28.
Yin, H., Ai, S., Shi, W., Zhu, L., 2009. Sens. Actuators B 137, 747–753.
Yu, J., Ju, H., 2002. Anal. Chem. 74, 3579–3583.
Yu, P., Zhou, H., Cheng, H., Qian, Q., Mao, L., 2011. Anal. Chem. 83, 5715–5720.
Yu, Y.-H., Soriano, A.N., Li, M.-H., 2009. J. Chem. Thermodyn. 41, 103–108.
Zhang, J., Lei, J., Liu, Y., Zhao, J., Ju, H., 2009. Biosens. Bioelectron. 24, 1858–1863.
Zhang, Y., He, P., Hu, N., 2004. Electrochim. Acta 49, 1981–1988.
Zheng, B., Xie, S., Qian, L., Yuan, H., Xiao, D., Choi, M.M.F., 2011. Sens. Actuators B 152, 49–55.
Zheng, W., Zheng, Y.F., Jin, K.W., Wang, N., 2008. Talanta 74, 1414–1419.
Zhou, G.-P., Zhang, Y., Huang, X.-R., Shi, C.-H., Liu, W.-F., Li, Y.-Z., Qu, Y.-B., Gao, P.-J., 2008. Colloids Surf. B 66, 146–149.
Zhou, Y., Zhi, J., 2006. Electrochem. Commun. 8, 1811–1816.
Zhu, H., Liang, X., Chen, J., Li, M., Zhu, Z., 2011. Talanta 85, 1592–1597.
Zhuo, Y., Chai, Y.-Q., Yuan, R., Mao, L., Yuan, Y.-L., Han, J., 2011. Biosens. Bioelectron. 26, 3838–3844.